Theoretical study on the removal function of computer controlled polishing SiC mirror with fixed abrasive

Xu Wang (王 旭)* and Ligong Zheng (郑立功)

Key Laboratory of Optical System Advanced Manufacturing Technology, Changchun Institute of Optics, Fine Mechanics and Physics, Chinese Academy of Sciences, Changchun 130033, China

**Corresponding author: wangxu-308@163.com*

Received September 20, 2011; accepted November 15, 2011; posted online April 27, 2012

A fixed abrasive technology combined with computer controlled optical surfacing is discussed, and a removal function model for multi-pellet polishing pad is established based on the removal function theory of planar motion. The parameters of the model, such as the movement eccentricity of the polishing pad and the distance between pellets, are optimized by introducing a approaching factor and a curve RMS distance in the simulation. The comparison of the theoretical model and the experimental results indicate that the error between the theoretical maximum removal rate and the experimental data is 0.0073 μm/ min, and its error ratio is 5.58%; the RMS distance error between the theoretical removal function curve and the experimental curve is 0.0849 μm and its error ratio is 7.01%. The veracity of the theoretical model is verified by experimental results, which predicts the feasibility of the fixed abrasive polishing technology and establishes a promising basis for the SiC mirror precision fabrication field.

OCIS codes: 220.0220, 220.4000, 220.4610, 220.5450.

doi: 10.3788/COL201210.S12201.

Fabricating the spherical and flat mirrors with the traditional slurry technology, the removal function of the polishing pad is not the preferential researching point, but on the research of the fabrication efficiency and the surface roughness. Golini *et al.* examined the physical mechanism of loose abrasive microgrinding[1]. Especially, they focused on the transition from brittle to ductile mode grinding.

The fixed abrasive technology developed in 1970s can offer several potential advantages over the slurry processes with pitch or polyurethane laps. These advantages[2] include polishing efficiency, temperature stability, cost of consumables, and compatibility with computer numerically controlled generating techniques. So the fixed abrasive becomes an alternative option to finish the optical mirrors. But the fixed abrasive technique also has its limitation, which is suitable for fabricating the middle and low steep aspherical mirrors. As for the high steep aspherical mirrors, MJT might be a good technique[3,4]. Some researchers studied the fabrication mechanism of the fixed abrasive in details, the work of Edwards *et al.*[5] was the most outstanding. They researched fine grinding mechanism (ductile cutting) using bound diamond abrasives, they found that the fracture mechanism was preferred to plastic scratching for most applications.

If applying the fixed abrasive technology to the practical engineering, especially to the fabrication field of aspheric mirrors, it is not enough that the research emphasis only on the material removal mechanism, also the material removal rate and surface roughness should be included. In this field, lots of engineers did the related work. Fletcher *et al.*[6,7] focused on the relationship between material removal rate and diamond grades (micron sizes of diamond). Bifano *et al.*[8] proved that the fixed abrasive is a viable fabrication process for high-performance aspheric mirrors by taking advantage of the relative ductility of ceramics compared with that of glass. In their another experiment[9], a 0.9-mm-thick ceramic hard disk substrates is finished to 8-nm RMS roughness and 8-μm flatness only with the fixed abrasive.

When fabricating the aspheric mirrors, the calculated amount material should be removed at calculated point on the mirror, which is called as deterministic fabrication. Hence the research on the removal function of the fixed abrasive polishing pad is much more important, especially the research on the shape and peak value of the removal function. The characteristic of the removal function is not only related to the characteristic of the used fixed abrasive pellets, but also related to the SiC material and the movement mode of the polishing pad. The starting point of this paper is different from others, the differences are shown as the combination of the fixed abrasive pellets and planar movement mode to polish the RB-SiC mirrors. The shape of the removal function depends on the movement mode of the polishing pad, and the peak value of the removal function and mirror surface roughness depends on the fixed abrasive material and the workpiece material. Finally, the fabrication result has a close relationship with the movement mode of the pad, the material of the pellets and the mirror. SiC material is a promising material for the large diameter, spaced telescope[10−12]. Our research establishes the technical basis for the fabrication of the large diameter, off-axis SiC mirror. In the letter, the researching process of the removal function peak value is combined with two-phase contacting model and the probability concept, and the researching process of the removal function shape includes the linear superposition concept and shape numerical optimizing concept.

The letter discusses the theoretical removal function of the fixed abrasive technology and also the related experiments are carried out to verify the model. The theoretical basis is established for fabricating SiC mirror with fixed abrasive.

In the process of fabricating SiC mirror, the planar motion (without self-rotation) is adopted for the working pad in our lab. So we aim at the removal function based on the planar motion of the polishing pad. The acquiring process of removal function is divided into two steps: the acquirement of the peak value and the acquirement of the function shape.

The pellets in experiment are composed of synthetic diamond abrasive and resin. The majority diameter of diamond particle is 5 μm, it obeys the Gaussian distribution. Supposing that the volume concentration of the diamond abrasive in the pellet is ξ (no unit, in percent form) and the diameter of the diamond abrasive is $\overline{D}$ (unit is μm), the abrasive number in the unit area on the surface of the pellet will be

$$m = \frac{4\xi^{2/3}}{\pi \overline{D}^2}. \tag{1}$$

The height of an abrasive outcropped from resin is a, which is in uniform distribution. Hence the distribution density function of a (uniform distribution) is

$$f(a) = \begin{cases} \dfrac{1}{a_{\max}} & (0 < a < a_{\max}) \\ 0 & (\text{other}) \end{cases}, \tag{2}$$

where $a_{\max}$ is the maximum outcropped height of one single diamond particle.

The distribution probability is the integral of the distribution density function, hence it is denoted as

$$P\{a < x\} = \int_0^x \frac{1}{a_{\max}} \mathrm{d}a = \frac{x}{a_{\max}}, \tag{3}$$

where $P\{a < x\}$ is the probability for one single abrasive whose outcropped height is less than certain value.

So the number of abrasives with height bigger than x in the unit area of pellet is

$$m_1 = m - m \cdot P\{a < x\} = \frac{4\xi^{2/3}}{\pi \overline{D}^2} \left(1 - \frac{x}{a_{\max}}\right). \tag{4}$$

In Ref. [13], the authors come to conclusion that the contact type between workpiece and abrasive is plastic deformation, while the contact type between working pad and abrasive is elastic deformation. The model in Ref. [13] and the principle of force balance are combined, the equation which describes the indentation depth into the RB-SiC workpiece by a particle of the diamond abrasive in pellet is obtained as follows[14]:

$$\delta_w^3 + \left(\frac{9H_w^2\pi^2\overline{D}}{8E_{fp}^2} - 3a\right)\delta_w^2 + 3a^2\delta_w - a^3 = 0, \tag{5}$$

where δ_w is the indentation depth into SiC workpiece by particle of diamond; E_{fp} is the equivalent Young's modulus of diamond abrasive and resin.

For single diamond abrasive, the material removal in time t is

$$\Delta G = k \cdot \Delta S \cdot V \cdot t, \tag{6}$$

where k is constant which is derived from Rabinowicz theory, its expression is given by

$$k = \frac{3}{\pi}\tan\theta \approx \frac{3}{\pi} \cdot \frac{\delta_w}{r} \approx \frac{3}{\pi} \cdot \frac{\delta_w}{\left(\overline{D}\delta_w\right)^{\frac{1}{2}}} = \frac{3}{\pi} \cdot \left(\frac{\delta_w}{\overline{D}}\right)^{\frac{1}{2}}, \tag{7}$$

t is the polishing time, ΔS is the cross section area of the groove in the workpiece formed by a single diamond abrasive, and V is the diamond abrasive instantaneous sliding velocity.

According to the definition of material removal rate, the expression of maximum removal rate is denoted as

$$\Delta Z = \frac{\Delta G N_a}{A_n t} = \frac{k \cdot \Delta S \cdot V \cdot N_a}{A_n}, \tag{8}$$

where N_a is the number of abrasives whose height is outcropped from the resin in area A_t, defined as $N_a = A_t m_1$. A_t is the total real contact area between the abrasive in the pellet and the workpiece, A_n is the macroscopic contact area between the pellet and the workpiece.

With the combination of Eqs. (4), (5), (6), and (8), finally the expression of maximum removal rate is obtained (derived details see in Eqs. (17)–(20) in Ref. [14]):

$$\Delta Z = \frac{12\xi^{2/3}}{\pi^2\overline{D}^2} V A_t^* \delta_w^2 \left(1 - \frac{x}{a_{\max}}\right), \tag{9}$$

where $A_t^* = A_t/A_n$.

The Preston function is a successful method to model the optical fabrication[7]:

$$\Delta Z(x, y) = K \cdot P(x, y) \cdot V(x, y), \tag{10}$$

where $\Delta Z(x, y)$ is the material removal at the point (x,y) in unit time; K is the coefficient which is related to the fabricating process, such as the working temperature, the polishing pad material type; $P(x, y)$ is the instantaneous pressure at point (x, y); $V(x, y)$ is the instantaneous relative velocity.

With the combination of Eq. (10) and the work of Wagner *et al.*[15], the normalized removal function of the working pad in unit time is given as

$$f(x, y) = \frac{1}{T(x, y)} K P(x, y) \int_{T(x,y)} V(x, y)\mathrm{d}t, \tag{11}$$

where $T\,(x, y)$ represents the whole polishing time at the point (x, y) in one polishing period, $P\,(x, y)$ is constant at every point for the entire period in assumption, also K is a constant which depends on the pressure, the relative velocity, and the material properties.

The sketch of the planar motion is displayed in Fig. 1, the polishing pad is without self-rotation, its orientation is fixed. r is the radius of polishing pad, e is the eccentricity, A is the random point on the workpiece. The area covered by polishing pad in one polishing period is centered at point O, its radius is $(r + e)$. The angle α is formed by line AO and y axis.

According to the movement characteristic of the polishing pad in planar motion, the expression of the angle α is

$$2\alpha = \begin{cases} 2\arccos\left(\dfrac{(x-m)^2+(y-n)^2+e^2-r^2}{2[(x-m)^2+(y-n)^2]^{1/2}\cdot e}\right) & r-e<[(x-m)^2+(y-n)^2]^{1/2}\leqslant r+e \\ 2\pi & 0\leqslant[(x-m)^2+(y-n)^2]^{1/2}\leqslant r-e \end{cases}, \tag{12}$$

where m is the x axis coordinate of the center point of the area formed by the motion of the single pellet, n is the y axis coordinate.

The random point on the workpiece has a invariable velocity to the polishing pad in the planar motion. The relative velocity equals ω times e. At meantime $\mathrm{d}t=\mathrm{d}\alpha/\omega$, with the combination of Eq. (11), the removal function of polishing pad is described as

$$f(x,y)=f(R)=\begin{cases} 2eKP\arccos\left(\dfrac{R^2+e^2-r^2}{2R\cdot e}\right) & r-e<R\leqslant r+e \\ 2\pi eKP & 0\leqslant R\leqslant r-e \end{cases}, \tag{13}$$

where $R=[(x-m)^2+(y-n)^2]^{1/2}$.

In the fixed abrasive technology, usually the working pad is composed of several pellets. The compositive removal function is the linear superposition of several pellets.

In the fabricating coordinates of the multi-pellet pad, the Eq. (13) is denoted as

$$f(R_i,m_i,n_i)=\begin{cases} 2eKP\arccos\left(\dfrac{R_i^2+e^2-r^2}{2R_i\cdot e}\right) & r-e<R_i\leqslant r+e \\ 2\pi eKP & 0\leqslant R_i\leqslant r-e \end{cases}, \tag{14}$$

where $R_i=[(x-m_i)^2+(y-n_i)^2]^{1/2}$, m_i, n_i are the coordinates of circle center formed by the movement of ith pellet. The coordinates of circle center formed by the planar motion of each pellet are calculated respectively.

According to the Eq. (10), the maximum material removal in time t is

$$\Delta W=\Delta Z\cdot t, \tag{15}$$

where ΔZ is the maximum removal rate in Eq. (9).

According to the Eq. (14), the maximum value of the removal function in time t is

$$|f(R_i,m_i,n_i)|_{\max}=2\pi eKP. \tag{16}$$

The expression of material removal is derived from two different ways they should be equal to each other, hence with the combination of Eqs. (15) and (16)

$$\Delta Z\cdot t=2\pi eKP. \tag{17}$$

Therefore, the Eq. (14) is denoted as

$$f(R_i,m_i,n_i,t)=\begin{cases} \dfrac{\Delta Z\cdot t}{\pi}\arccos\left(\dfrac{R_i^2+e^2-r^2}{2R_i\cdot e}\right) & r-e<R_i\leqslant r+e \\ \Delta Z\cdot \mathrm{t} & 0\leqslant R_i\leqslant r-e \end{cases}, \tag{18}$$

where $\Delta Z=\frac{12\xi^{\frac{2}{3}}}{\pi^2D^2}VA_t^*\delta_w^2\left(1-\frac{x}{a_{\max}}\right)$.

Finally, the removal function of multi-pellet polishing pad can be denoted as

$$F=\sum_{i=1}^{n}f(R_i,m_i,n_i,t). \tag{19}$$

Equation (19) is the final expression of removal function which includes several main fabricating parameters.

The desired removal function shape is with a central peak results in successful figuring, and with a smooth fall off. The width of the function determines how rapidly the desired surface figure is achieved. If the central region of the removal function is approaching the Gaussian function with a narrow width, the mirror surface error will decrease rapidly[16,17].

For a better removal function shape, the 7-pellet polishing pad[18] is adopted in the experiment. The sketch of pellets distribution is shown in Fig. 2.

The pellet material are resin, the particle material in pellet is diamond, the diameter is 5 μm. The pellet diameter is 10 mm, the thickness is 5 mm, the pellet surface is flat.

The parameter d is the distance between the center points of pellets. The parameter e is the eccentricity of the polishing pad. The three-dimensional removal function is rotational symmetric in planar motion mode, for the sake of it, the data on cross section are representative and picked up. To evaluate the removal function, the

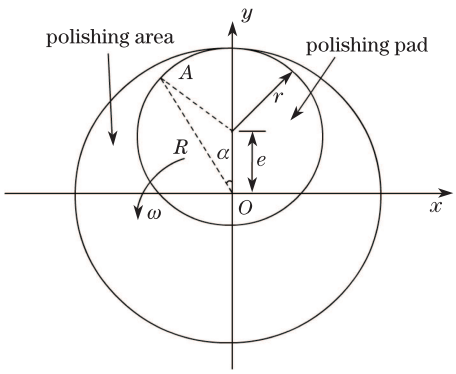

Fig. 1. Principle map of planar motion, $R = [(x-m)^2 + (y-n)^2]^{1/2}$.

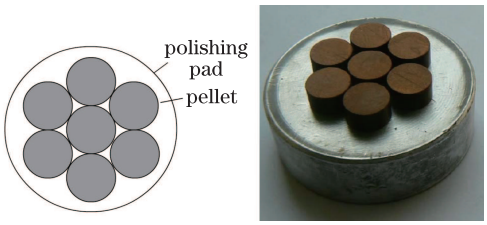

Fig. 2. Distribution of pellets.

approaching factor and the curve rms error are introduced into the paper.

The definition of the approaching factor is the ratio of $W_{1/4}$ to the whole removal W. W is the total removal in the whole polishing area. $W_{1/4}$ is the removal in the circle with shadow whose radius is 1/4 of the whole polishing area radius. The approaching factor represents the relationship between the three-dimensional removal function and the three dimension Gaussian function. The bigger the approaching factor is, the stronger the ability of the removal function is, and much more approaching the Gaussian function the removal function is.

Its expression is[19]

$$F_{1/4} = \frac{W_{1/4}}{W}. \tag{20}$$

According to the definition of the approaching factor and the Eq. (19), the numerical relationships are calculated, the details are displayed in Table 1.

The definition of the curve RMS error is the root mean square of the simulated normalized removal function and a Gaussian function with certain μ and σ. The rule of calculating μ and σ are as follows: the peak value of the Gaussian function is equal to the simulated removal function's, the value at the edge of simulated removal function is equal to the value of the Gaussian function at 3σ. For the most situations, μ is equal to 0. The curve RMS error represents the matching degree between the removal function and the Gaussian function. The less the error, the higher the matching degree.

The curves RMS error is denoted as

$$D_{\mathrm{RMS}} = |f_1 - f_2| = [(f_1 - f_2)^{\mathrm{T}} (f_1 - f_2)]^{1/2}, \tag{21}$$

where f_1 is the simulated removal function, and f_2 is the Gaussian function. It represents the "distance" between f_1 and f_2.

According to the definition of the curve RMS error and the Eq. (19), the numerical relationships are calculated, the details are displayed in Table 2.

The bigger the data in Table 1, the more optimized the simulated removal function. The smaller the data in Table 2, the more approaching a Gaussian function the simulated removal function. In Table 1, the most optimized data is e=9 mm, d=10 mm. In Table 2, the most optimized data is e=9 mm, d=10 mm.

Aiming at a better experimental result, the experimental specifications are all based on the parameters optimized before.

The pellet abrasive size is W5. The pellet diameter is 10 mm, its thickness is 5 mm, the pellet concentration is 10%, the resin type is SP27C, the pellet surface type is flat.

The SiC workpiece is manufactured by Changchun Institute of Optics, Fine Machines and Physics, Chinese Academy of Sciences (CIOMP), its length is 205 mm, the width is 125 mm . The workpiece picture is shown in Fig. 3(b). All the experiments are carried out on this SiC workpiece.

The fabrication equipment is FSGJ-1 (acronym of Chinese spell) computer controlled grinding/polishing

Table 1. Numerical Relationship between $F_{1/4}$ and d, e. (The unit of d and e is mm, the unit of middle data is μm)

d	e				
	11	10	9	8	7
10	0.1388	0.1477	0.1492	0.1468	0.1331
12	0.1374	0.1369	0.1219	0.1135	0.1087
14	0.1145	0.1057	0.1002	0.0906	0.0806

Table 2. Numerical Relationship between Curve RMS Error and d, e. (The unit of d and e is mm, the unit of error data is μm)

d	e				
	11	10	9	8	7
10	0.1097	0.1076	0.0691	0.0707	0.0813
12	0.1162	0.0900	0.0796	0.1521	0.2769
14	0.0862	0.1371	0.2693	0.3771	0.3999

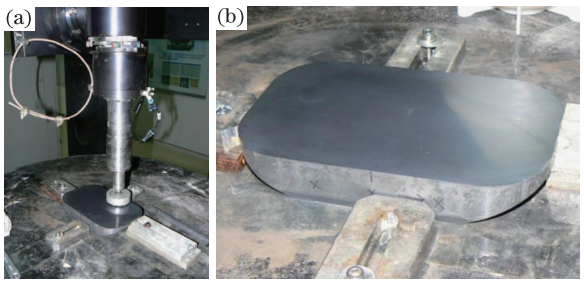

Fig. 3. (a) Experimental picture. (b) SiC workpiece picture.

machine manufactured by our own laboratory. The mechanical structure of the machine is only designed for the planar motion mode. Its fastest rotation speed is 200 rpm, the maximum of pressure intensity is 0.5 MPa, and the limit of eccentricity is 10 mm. The experimental picture is shown in Fig. 3(a).

Firstly, the SiC mirror surface is tested and saved with interferometer. The surface data are set to be the reference data, the mirror position is marked and saved. In the next step, the fixed area on the SiC mirror is polished by the machine FSGJ-1. The rotation speed is set to be 200 rpm (maximum), the pressure intensity is also set to be 0.5 MPa (maximum), the time of one fabricating period is 360 s. After one fabricating period, the SiC mirror is retested with interferometer, and the Sys Err File function (It is a functional module in MetroPro interferometer software from Zygo company, it is able to calculate the error between two tests) is used to obtain the surface error between two tests. The error data of two tests are the result of the removal function in 360 s. The process is repeated four times, four data are obtained. The PV values of the profile on cross section are interested and focused on. These data are given in Table 3.

The concentration of used pellets is 10%, with the combination of experimental parameters and Eqs. (5) and (9), the calculation result of simulated peak removal rate of the polishing pad is $\Delta Z_{\text{theory}} = 0.1309$ μm/ min. The experimental result of the peak removal rate is $\Delta Z_{\text{experiment}} = 0.1237$ μm/ min. The ratio of error between simulation and experiment is

$$\beta = \frac{\Delta Z_{\text{theory}} - \Delta Z_{\text{experiment}}}{\Delta Z_{\text{theory}}} = 5.58\%.$$

For intuitionistic comparison, the simulated and experimental removal functions are plotted in the same coordinates. The result is shown in the Fig. 4.

The comparison of wavefront maps are shown in the Fig. 5.

To evaluate the similarity of Fig. 5, the concept of structural similarity (SSIM)[20] is introduced into the paper,

$$\text{SSIM}(x, y) = \frac{(2\mu_x\mu_y + C_1)(2\sigma_{xy} + C_2)}{(\mu_x^2 + \mu_y^2 + C_1)(\sigma_x^2 + \sigma_y^2 + C_2)}, \qquad (22)$$

where the mean intensity μ_x, μ_y are given by $\mu_x = \frac{1}{N}\sum_{i=1}^{N} x_i$, $\mu_y = \frac{1}{N}\sum_{i=1}^{N} y_i$.

The standard deviation (the square root of variance) are given by

$$\sigma_x = \left[\frac{1}{N-1}\sum_{i=1}^{N}(x_i - \mu_x)^2\right]^{\frac{1}{2}},$$

$$\sigma_y = \left[\frac{1}{N-1}\sum_{i=1}^{N}(y_i - \mu_y)^2\right]^{\frac{1}{2}},$$

$$\sigma_{xy} = \frac{1}{N-1}\sum_{i=1}^{N}(x_i - \mu_x)(y_i - \mu_y).$$

The constant C_1 is included to avoid instability when $\mu_x^2 + \mu_y^2$ is very close to zero, the constant C_2 is included to avoid instability when $\sigma_x^2 + \sigma_y^2$ is very close to zero.

The calculation result is SSIM=0.8690, which means the similarity of simulated and experimental removal functions is 86.90%.

The curve RMS error of simulated and experimental curves in Fig. 4 is $D_{\text{RMS}} = 0.0849$ μm, the ratio of RMS error to the maximum simulated removal rate is

$$n = \frac{D_{\text{RMS}}}{|f_{\min}|} = 7.01\%, \qquad (23)$$

where $f_{\min}$ is the value at the peak or the valley of the removal function.

The results obtained are analyzed as follows:

(1) The experimental removal rate is a little lower than the simulated removal rate. The insufficient ability of breaking-in is the main cause of the result. The worn diamond particles cannot fall off in time, which causes the lower cutting efficiency. In addition, under the same pressure, the indentation into the RB-SiC workpiece by a diamond particle is supposed to be δ_w in the simulation according to the Eq. (5). But as the matter of the fact, there will be lots of indentation formed by diamond particles lower than δ_w due to the poor uniformity of abrasive diameter. The situations mentioned above are the obvious causes that the experimental removal rate is

Table 3. PV Values of the Profile on Cross Section

	1	2	3	4	μ	σ
λ	1.2560	1.2420	1.0360	1.1560	1.1725	0.1012
μm/ min	0.1325	0.1310	0.1092	0.1219	0.1237	0.0107

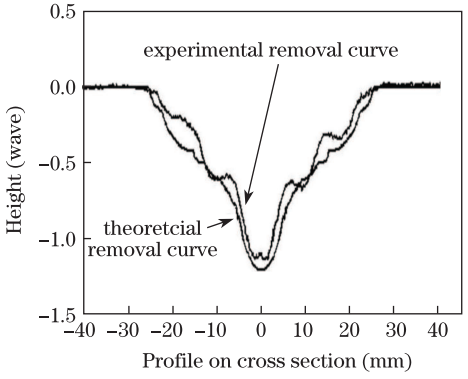

Fig. 4. Comparison of theoretical and experimental removal function.

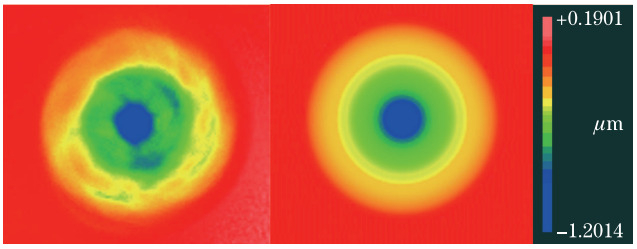

Fig. 5. Surface/wavefront map comparison of experimental removal function (left) and theoretical removal function (right).

lower. Therefore the binding force of resin and diamond particles should be optimized in producing the pellets, and the uniformity of abrasive diameter should be improved.

(2) The obvious "step effect" of the removal function emerges. The curve of the removal function with step effect is not very smooth. Though the curve is continuous, the derivative function of the curve is not smooth. Several obvious inflexions exist on the removal function curve which can introduce middle spatial frequency to the mirror surface.

For the sake of it, the filling factor is introduced to evaluate the step effect. The factor is defined as the ratio of the working contact area of pellets to the circle contour area formed by the outer pellets. The equation is

$$\mu = \frac{S_{\text{contact}}}{S_{\text{contour}}}, \tag{24}$$

where S_{contact} is the contact area between the pellets and the workpiece; S_{contour} is the contour area formed by the outer pellets of the polishing pad.

The step effect reflects the spatial frequency error of the polishing pad. The spatial frequency of the pad can be reproduced to the mirror surface when polishing the SiC workpiece. Therefore a slighter step effect is the key factor of obtaining a better mirror with less ripples. Increasing the filling factor is an effective solution for reducing the step effect.

In conclusion, the removal function shape model of multi-pellet pad is founded based on the planar motion of the pad. The shape model and the removal rate model form the complete removal function model. Series of simulations are verified by the experiments, which confirms the validity of the removal function model. The experimental results indicate that the removal rate error of simulation and experiment is 0.0073 μm/ min, the ratio of error is 5.58%, and the removal function curve error of simulation and experiment is $D_{\text{rms}} = 0.0849$ μm, the ratio of error is 7.01%. The comparison results illuminate that under a certain conditions, the removal function of grinding/polishing the SiC mirror with the fixed abrasive is stable and predictable in one fabricating period, which establishes the basis of the determinate fabrication of SiC mirror.

This work was supported by the Fund of "Study on the basic theory and key techniques of space optical fabrication and metrology" under Grant No. 2011CB01320005.

References

1. D. Golini and S. D. Jacobs, Appl. Opt. **30,** 2761 (1991).
2. B. E. Gillman and S. D. Jacobs, Appl. Opt. **37,** 3498 (1998).
3. C. Shi, J. Yuan, F. Wu, X. Hou, and Y. Wan, Chin. Opt. Lett. **8,** 323 (2010).
4. C. Shi, J. Yuan, F. Wu, and Y. Wan, Chin. Opt. Lett. **9,** 092201 (2011).
5. D. F. Edwards and P. P. Hed, Appl. Opt. **26,** 4670 (1987).
6. T. D. Fletcher, B. Dronen, F. T. Gobena, and E. Larson, Presented at Optifab 2003, Rochester, New York, May 2003.
7. T. Fletcher, F. Gobena, and V. Romero, in *Proceedings of OSA Optical Fabrication and Testing Topical Meeting, Rochester NY* (2010).
8. T. Bifano, Y. Yi, and W. K. Kahl, Precision Engineering **16,** 109 (1994).
9. T. G. Bifano and P. A. Bierden, Tools Manufact. **37,** 935 (1997).
10. W. J. Choyke, R. F. Farich, and R. A. Hoffman, Appl. Opt. **15,** 2006 (1976).
11. K. Enya, T. Nakagawa, and H. Kaneda, Appl. Opt. **46,** (2007).
12. S. J. Kishner, G. J. Gardopee, and M. B. Magida, Proc. SPIE **1335,** 127-139 (1990).
13. Y. Zhao and L. Chang, Wear **252,** 220 (2002).
14. X. Wang and X. Zhang, Appl. Opt. **48,** 904 (2009).
15. R. E. Wagner and R. R. Shannon, Appl. Opt. **13,** 1683 (1974).
16. R. A. Jones, Appl. Opt. **16,** 218 (1977).
17. R. A. Jones, Appl. Opt. **18,** 1244 (1979).
18. W. Zheng, T. N. Cao, and X. Z. Zhang, Proc. SPIE **4231,** 51 (2000).
19. Y. Wang and J. C. Yu, Opt. Technique (in Chinese) **29,** 258 (2003).
20. Z. Wang, A. C. Bovik, H. R. Sheikh, and E. P. Simoncelli, IEEE Trans. Image **14,** 600 (2004).